Atomic Scale Investigation of Structural Properties and Glass Forming Ability of $Ti_{100-x}Al_x$ Metallic Glasses

M. TAHIRI, A. HASNAOUI, and K. SBIAAI

In this work, we employed molecular dynamics (MD) simulations to study Ti-Al metallic glasses (MGs) using the embedded atom method (EAM) potential to model the atomic interaction with different compositions. The results showed evidence of the metallic glass formation induced by the split occurring in the second peak of the radial distribution function (RDF) curves implying both Ti and Al atoms. The common neighbor analysis (CNA) method confirmed the presence of the icosahedral clusters with a maximum amount observed for an alloy with 75 pct of Al. Analysis of coordination numbers (CNs) indicated that the total CNs are nearly unchanged in these systems. Finally, Voronoi tessellation analyses (VTA) showed a higher value of the number of icosahedral units at $Ti_{25}Al_{75}$ composition. This specific composition represents a nearby peritectic point localized at a low melting point in the Ti-Al binary phase diagram. The glass forming ability (GFA) becomes important when the fraction of Al increases by forming and connecting "icosahedral-like" clusters (12-coordinated $\langle 0, 0, 12, 0\rangle$ and 13-coordinated $\langle 0, 1, 10, 2\rangle$) and by playing a main role in the structure stability of the Ti-Al MGs.

https://doi.org/10.1007/s11661-018-4541-3

I. INTRODUCTION

SEVERAL research studies concentrated on investigating the structural properties in metallic glasses (MGs)[1–4] that require particularly high cooling rates. MGs have received great consideration mainly due to their outstanding mechanical strength, thermal, and chemical attributes.[5] The retention of this amorphous structure of MGs occurs when a liquid metal undergoes a fast quenching. However, the formation of MGs is favorable by respecting the rules of Inoue[6] for good glass forming ability (GFA). He proposed that the formation of MGs requires a significant difference in atomic size ratios (above 12 pct), a multicomponent material, and the presence of a eutectic point in the phase diagram. For some systems, the cooling rate required to form the metallic glass structure is very high and sometimes is not easy to reach through experimental methods. These very high cooling rates are easily reachable *via* molecular dynamics (MD) simulations. Besides, this simulation technique does not only reveal the structural sides of the metallic glass formation but also sheds light on the forming ability of the studied system.[7] Most prominently, MD simulations can give a better understanding and control of quantities that are difficult to determine in real experiments with a good precision. There are many studies dealing with MD simulations of the formation of MGs and their structural properties such as Al-Mg,[8] Cu-Zr,[9] and Ti-Al.[10–12] Most of these works investigated the glassy state of binary and ternary systems during the cooling process using different techniques such as energy/volume change, radial distribution functions (RDFs), coordination numbers (CNs), and common neighbor analysis (CNA). Wang and Wong[8] studied a wide range of compositions of Al-Mg amorphous structure using MD simulations where the interatomic interactions were described by the embedded atom method (EAM) potential. The simulation showed that Mg atoms are more likely to serve as neighbor atoms in Al-centered icosahedral clusters for the middle concentrations or to form larger polyhedra at the Al-rich side of the phase diagram. The Voronoi tessellation analyses (VTA) showed that Al-centered icosahedra are abundant for most compositions of the Al-Mg alloy. The presence of a high number of 155-type pairs proves that icosahedral arrangement is dominant for all compositions of the Al-Mg alloys with some differences in the topological arrangement of the different clusters. The medium-range order (MRO) was attributed to connected icosahedra that share atoms to constitute a cluster network.

M. TAHIRI, A. HASNAOUI, and K. SBIAAI are with the Laboratoire LS3M, Faculté Polydisciplinaire Khouribga, Univ Hassan 1, 25000 Khouribga, Morocco. Contact email: mmounirtahiri@gmail.com

Manuscript submitted August 5, 2017.
Article published online March 19, 2018

Xie *et al.*[10] used MD simulations in order to examine the evolutions of Frank–Kasper polyhedra during the supercooling process of $TiAl_3$ alloy. They observed the occurrence of a spilt in the second peak in the RDF curve, which they attributed to the formation of the metallic glass. They also noticed that further relaxation for 50 ns at the glass transition temperature T_g significantly enhanced the amount of these clusters and their connectivity with other clusters. They also concluded that the length of the relaxation time has an effect on improving the growth of these clusters.

Other MD simulations[11] examined the characteristics of icosahedral clusters in TiAl alloy with different cooling rates. They found that the high cooling rate plays an important role in the evolution of icosahedral clusters and linked it to the glass transition temperature. Furthermore, the authors suggested that the MROs of icosahedral clusters have a good structural stability. They concluded that the formation of icosahedral clusters is a barrier to crystal nucleation in supercooled liquid metals.

Wang and Wong[13] investigated the supercooled liquid $Zr_xCu_{90-x}Al_{10}$ by varying Zr composition extending from 20 to 70 pct. Radial distribution functions were used to determine correlations between different atom pairs and the corresponding interatomic distances at the short-range order (SRO). The CNs study showed that the total CN is nearly invariant in these systems under the composition variation. It has been found that Cu atoms have a tendency to form smaller clusters, while Zr atoms tend to form larger clusters. Finally, CNA revealed a good GFA by the addition of a low Al concentration to Zr-Cu alloys.

Aluminum-based MGs are potentially classified among the most interesting MGs, mainly due to their outstanding mechanical strength and exceptional corrosion resistance in comparison to their crystalline counterpart.[14–17] Unfortunately, the glass-forming ability (GFA) of Al-based alloys is particularly low and the critical size for glass formation reached so far is modestly of the order of 1 mm.[18] The glass transition was not possible without prominently high cooling rates because of the low GFA in Al-based alloys. In addition to a significant atomic size mismatch, the alloy composition may influence the GFA "a degree of the ease of vitrification," as suggested by Inoue.[6] Such studies should shed light on the choice of the elements and the proportions to form stable MGs. The $Ti_{100-x}Al_x$ alloy is carefully chosen in this work for its large atomic size difference, $R_{Al} = 1.18$ Å and $R_{Ti} = 1.76$ Å, making it a potential candidate for forming MGs. Furthermore, many compositions will be investigated to highlight the entire evolution of clusters.

Within the last few years, TiAl alloys have received much consideration due to their outstanding properties characterized by high specific strength and exceptional resistance at high temperatures. TiAl is considered as the next innovating structural material mainly in the aerospace and automotive industries.[19–22] The glass transition process is a very valuable technique to improve the performance of material properties of Ti-Al alloy.[23] Glassy alloys are commonly considered as the state of frozen liquids; however, the difference in their structure is obvious. As discussed in our previous studies,[24,25] a split occurred in the second peak of the radial distribution function curve for $TiAl_3$ MG. This splitting of the second peak is a distinguished characteristic of metallic glass formation. Thus, quenching the Ti-Al alloy from the liquid to 300 K at different cooling rates (5×10^{12}, 10^{13}, and 10^{14} K/s) leads to a metallic glass. To our knowledge, there has been no systematic and full investigation of clusters and their configurations in the Ti-Al system with different compositions. In this article, MD simulations with EAM potential were employed to investigate the composition effect on the GFA of Al-Ti alloys. Different techniques, such as RDFs, CNs, CNA, and VTA, were used. In Section II, we present the computational technique used. In Section III, we display and analyze our results. In Section IV, we present our conclusions.

II. COMPUTATIONAL DETAILS

The MD simulations were performed on $Ti_{100-x}Al_x$ systems using the large-scale atomic/molecular massively parallel simulator (LAMMPS)[26,27] and by employing the EAM potential to model the atomic interaction. The simulation cells consist of 5324 Ti/Al atoms in a cubic box. Initially, different box sizes (between 2000 and 12,000 atoms) were used and showed that a size of around 4000 to 5000 atoms is a very satisfying value to save the computation time with keeping low enough statistical errors. In different alloy compositions of the $Ti_{100-x}Al_x$ systems, x spans the following values: 0, 15, 25, 38, 50, 63, 75, 90, and 100. The equations of motion are numerically integrated using the Verlet algorithm with a time-step of 1 femtosecond (fs). The temperature and pressure are controlled using a Nose–Hoover thermostat and barostat.[28] All the systems were first heated at a rate of 5×10^{12} K/s, from 300 K to 2500 K using an NPT ensemble to allow volume change. The end temperature 2500 K is chosen to be higher than the melting temperatures of the alloy systems. In order to allow atoms to diffuse and forget their initial positions, we equilibrate the structure in the liquid phase using an NVT ensemble at 2500 K for 100 ps. This procedure ensures having a liquid state for all the considered compositions. Then all systems were cooled from the liquid state to reach 300 K, using an NPT ensemble with a cooling rate 5×10^{12} K/s. Configurations and atom coordinates were stored at each equilibration stage for further studies with an interval of 100 K during the rapid solidifications. For MD simulations, the use of integrators with a correct convergence of the finite difference scheme dictates using a time-step in the femtosecond scale, typically 1 to 2 fs. Thus, a one million iteration simulation corresponds to a physical time of only 1 ns. Therefore, large systems including several millions of atoms will be treated only at the nanosecond timescale. In the context of MG formation, the MD limitation induces the use of very high cooling rates (typically of the order of 10^{11} to 10^{14} K/s) whose

magnitude orders are larger than what is used experimentally. However, some systems are hard to vitrify experimentally and need to be cooled in an extra fast way, implying rates of the order of those used in MD simulation. It turns out that the timescale limitation of MD simulations would be an advantage in this case, allowing the vitrification of a large variety of systems including monoatomic metals.

In this study, we adopted the EAM potential to describe the interatomic interactions between the atoms of the Al-Ti alloy. This interatomic potential consists of a simple embedding energy function and a short-range pairwise potential function and is given by[29,30]

$$E_{\text{tot}} = \sum_i F_i(\rho_{h,i}) + \frac{1}{2}\sum_{i \neq j} \phi_{i,j}(R_{ij}) \quad [1]$$

where $\phi_{i,j}$ is the short-range pair potential and R_{ij} is the distance between atoms i and j. The host density $\rho_{h,i}$ is approximated by the superposition of atomic densities ρ^{α}, *i.e.*, $\rho_{h,i} = \sum_{i \neq j} \rho_j^{\alpha}(R_{ij})$. Here, ρ^{α} is the contribution to density from atom j. Therefore, in essence, energy is a simple function of the positions of atoms.

In this work, we use the EAM interatomic potential of the Ti-Al system developed by Zope and Mishin, whose parameters are determined in Reference 31.

Structure analysis of the simulated Ti-Al system was performed using the radial distribution function $g(r)$, the CNA, the CN, and the VTA. The $g(r)$ function is expressed as

$$g(r) = \frac{V}{N^2}\left\langle \sum_{i=1}^{n} \frac{n(r)}{4\pi r^2 \Delta r} \right\rangle \quad [2]$$

where N denotes the number of atoms in the simulation cell, V is the volume of the cell, and $n(r)$ is the number of particles, which can be found in the shell from r to $r + \Delta r$. For binary alloys, the partial radial distribution functions for atoms α and β are computed by

$$g_{\alpha\beta}(r) = \frac{V}{N_\alpha N_\beta}\left\langle \sum_{i=1}^{N_\alpha} \frac{n_{i\beta}(r)}{4\pi r^2 \Delta r} \right\rangle \quad [3]$$

We also employed the CNA proposed by Clarke and Jónsson.[32] According to this technique, each pair of nearest-neighbor atoms is given by three indices jkl, where the first index j is 1 when two atoms are bonded to each other and is 2 if they are not. The second index k is the number of common nearest neighbors shared by the two atoms, and the third index l is the number of bonds among the shared neighbors. The CNA method can effectively detect various local atomic arrangements. For example, a CNA index of 555 corresponds to a pentagonal bipyramid, which is the building block of an icosahedron,[33] while 421 and 422 are the characteristics of fcc and hcp structures, respectively. For a liquid state, a low CN value is commonly found, while for MGs, with strong metallic bonding and dense packing, a high CN is expected.[34,35] To determine the bonding preferences of the different elements, the $g(r)$ functions were integrated to generate the various atomic CNs. In both techniques, a cutoff value of the first shell was set as the minimum after the first peak of the corresponding $g(r)$ function.

VTA involve the decomposition of the system into a finite amount of polyhedra centered near the various atomic sites, with volumes encompassed by each polyhedron consisting of the set of all points closer to that given atomic center than any other. We also made use of the Voronoi tessellation method to identify the number n_i of i-edged ($i = 3, 4, 5, 6, \ldots$) faces in a Voronoi cell by the indices $< n_3, n_4, n_5, n_6 >$. An i-edged face reflects the local symmetry of the solute atom with some nearest-neighboring atoms in a certain direction, as discussed in detail in Reference 36. For example, the ideal icosahedron is represented as $\langle 0, 0, 12, 0 \rangle$. If one 155-type pair is broken, it will result in a distorted icosahedron with a Voronoi index such as $\langle 0, 2, 8, 2 \rangle$. Note that the sum of the four indices determines the GFA of each atom.

III. RESULTS AND DISCUSSION

All the studied samples were checked after the heating stage and showed evidence for a liquid state by analyzing the $g(r)$ function that was found to possess the features of a liquid $g(r)$ curve. The obtained liquids were then cooled to room temperature (300 K) at the aforementioned cooling rate to form the metallic glass structure, as described in Section II. The resulting metallic glass was relaxed at 300 K with zero pressure in the canonical (NPT) ensemble for 100 ps.

A. *Radial Distribution Function*

The radial distribution function analysis is one of the most suitable methods to reveal the structure features of complex material. We investigate a wide range of compositions of the Ti-Al alloys. Partial and total $g(r)$ were employed to study the atomic arrangement. Figure 1(a) shows the total $g(r)$ function of the $Ti_{100-x}Al_x$ systems at 300 K obtained with a cooling rate of 5×10^{12} K/s. The $g(r)$ functions of all the considered alloys exhibit a distinct first peak for which the radial position shifts from 2.84 Å for pure Al glass to 2.87 Å for pure Ti glass. The assessed radius of Al atoms is smaller than that of Ti atoms. Therefore, the simulations give a slight growing radial distance value when the concentration of atoms with the larger radius increases. This behavior is in agreement with a previous study performed on Al-Mg alloy.[8] For the Ti-rich zone ($x = 0$, $x = 15$, and $x = 25$), the $g(r)$ function shows few peaks that are synonymous to some crystal-like features as the timescale is very short, crystallization could not be complete, but there is an obvious indication of its occurrence at least partially (Table I). We also observed that as the concentration of Al increases, the first peak of the total $g(r)$ function decreases in amplitude. When the Al concentration reaches 38 pct, the second peak of the $g(r)$ function begins clearly to split into two subpeaks that are more pronounced in the

Al-rich zone. The result of the splitting of the second peak is a notable characteristic of MGs and agrees quite well with previous investigations of the solidification of Ti-Al alloys[12] with a cooling rate of 10^{11} K/s, especially when the Al concentration exceeds 50 pct. However, RDF curves obtained by using a cooling rate of 5×10^{12} K/s display few peaks for the Ti-rich zone (Figure 1(a)), which we attribute to incomplete crystallization.

This splitting of the second peak is also perceived in the partial $g(r)$ function of Ti-Al alloys (Figures 1(b) through (d)). This means that both Ti and Al atoms participate in the metallic glass activity of our alloys, as has been observed in some compositions in previous simulation works performed on $TiAl_3$[24,25] and TiAl.[11] Moreover, our results agree with those obtained by experimental techniques (X-ray diffraction, extended X-ray absorption fine structure, and neutron diffraction) that have been applied for studying the microstructure of MGs[37–39] and linked the splitting of the second peak in partial radial distribution functions (PRDFs) to the glass transition.

Furthermore, the CNA confirms the aforementioned results by detecting the presence of icosahedral structural units. The maximum of the icosahedral cluster amount (10 pct) is reached for an Al concentration of 75 pct and then drops when the Al concentration reaches 90 pct (Table I). The maximum number of icosahedral units obtained during the rapid solidification process is found to be at the $TiAl_3$ composition, which is in agreement with a previous study[12] where the growth capability of icosahedral units with temperature was found to be higher for the $TiAl_3$ alloy than the other compositions. This specific composition of 75 pct of Al characterizes a nearby peritectic point in the Ti-Al binary phase diagram, confirming the condition of Inoue[6] suggesting that specific points in the phase diagram promote GFA. Some works[40] reported a value close to 60 pct of icosahedral units; this is not in contradiction with our results since we count only the centered atoms in the icosahedral unit,[24,25] while these works consider all the atoms involved in the icosahedral cluster.

We note also that the intensity of the first peak in the Al-Al partial $g(r)$ function increases with the increase of Al concentration, while that corresponding to Ti-Ti decreases. This is related to the abundant Al-Al bonds, which are attributed to the high probability of finding Al atoms localized within the radial distance from a centered Al atom.

B. *Coordination Numbers*

To investigate the first neighborhood shell for the atoms, we computed the CNs of the different atoms. We used a cutoff distance corresponding to the first minimum of the corresponding $g(r)$ function since the average coordination can be obtained by integrating the first $g(r)$ peak. For the Ti-Ti, Al-Al, and Ti-Al pairs, the considered cutoff values were 3.87, 3.68, and 3.86 Å, respectively, and did not change significantly with varying composition. Table II illustrates the total and partial CNs for Ti-Al alloys. We observe that the average CN_{all} remains nearly constant at around 13 despite the changes in composition. This coordination differs from the coordination of the crystalline structure CN = 12, which means that the structure was altered and could be distorted or changed completely. The GFA of Ti atoms CN_{Ti} and that of Al atoms CN_{Al} generally increase with increasing Al concentrations. However, CN_{Ti} is larger than CN_{Al} for all considered compositions. This is consistent with the difference in atomic radius (R_{Ti} = 1.76 Å, R_{Al} = 1.18 Å). Larger atoms possess more neighbor space, which can accommodate more neighbor atoms. The partials $CN_{Al\text{-}Al}$ (the number of Al atoms surrounding an Al atom) and $CN_{Ti\text{-}Al}$ (the number of Al atoms surrounding a Ti atom) increase with the increase of Al concentration, while those corresponding to $CN_{Ti\text{-}Ti}$ and $CN_{Al\text{-}Ti}$ drop. This behavior is consistent with a study done on Al-Mg[8] and Zr-Cu-Al[13] MGs. This can be explained by the abundance of the bounds that the Al atoms form when their concentration increases.

For more details, we plot in Figure 2 the distribution of major total CNs in the nearest neighbor of each atom type in the Ti-Al MGs at 300 K as a function of Al composition. In Figure 2, we illustrate the distribution of total CNs, and we find that in Al-Ti MGs, the 12-, 13-, 14-, and 15-coordinated atoms are the most abundant, with their fractions varying from 10 to roughly 50 pct.

We observe from this figure that the behavior of these CNs can be divided into two main parts. (1) For Al compositions lower than 25 pct, the 12- and 13-coordinated atoms are the predominant ones forming almost 80 pct of the metallic glass clusters. The 14-coordinated atoms constitute almost 12 pct of the system, while all the other CNs are not significant. (2) For Al compositions larger than 25 pct, we observe that the number of 15-coordinated atoms becomes important and reaches 10 pct, while the amounts of 12- and 13-coordinated atoms decrease to reach 30 pct.

We note that the icosahedral clusters are suggested to be the building blocks of a large variety of MGs at the SRO, while their connecting network should provide the MRO structural feature. In their ideal form, the icosahedra are 12-coordinated clusters, but they can show a defect form with a 13-coordinated cluster. In this context, we think that the increase of 12- and 13-coordinated clusters should be linked to the formation of icosahedral structural units, which is believed to promote the glass formation. Wang and Wong[13] studied the formation of Zr-Cu-Al metallic glass and found that the high fraction of atoms with CN = 12 in the Cu-rich zone facilitates the development of icosahedral structure in Zr-Cu-Al systems. Furthermore, we suggest that the increase of the higher coordinated atoms CN = 14 and 15 should lead to more dense clusters increasing the atomic packing factor of the material, which should increase the forming ability of the metallic glass.

For a more detailed study, we computed the atomic CNs for each central atom (Al and Ti) and plotted the results in Figure 3. We see from this figure that when increasing the Al composition, the CNs around Al

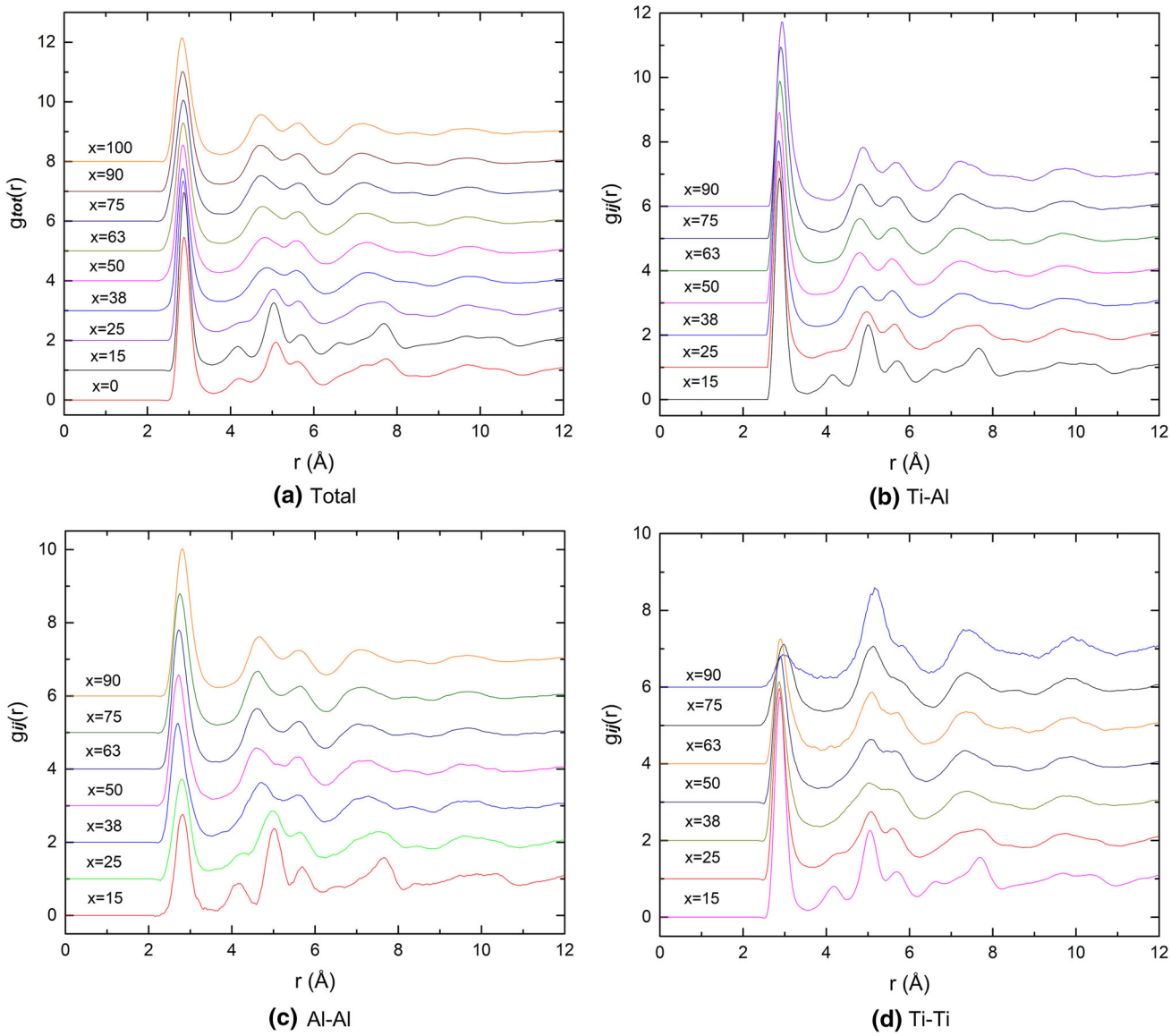

Fig. 1—(*a*) Total $g(r)$ function for $Ti_{100-x}Al_x$ systems and partial $g(r)$ functions for (*b*) Ti-Al, (*c*) Al-Al, and (*d*) Ti-Ti of the Ti-Al MGs at 300 K obtained using a cooling rate of $5{\cdot}10^{12}$ K/s. Individual curves correspond to different alloy compositions, as given in the figure. All curves were shifted vertically for clarity.

Table I. Evolution of Icosahedral Structure in Ti-Al Alloys at 300 K with the Cooling Rate of $5{\cdot}10^{12}$ K/s

Systems	$Ti_{85}Al_{15}$	$Ti_{75}Al_{25}$	$Ti_{62}Al_{38}$	$Ti_{50}Al_{50}$	$Ti_{37}Al_{63}$	$Ti_{25}Al_{75}$	$Ti_{10}Al_{90}$
Others (Pct)	64.50 ± 1.09	93.90 ± 1.31	96.60 ± 1.25	94.40 ± 1.32	92.00 ± 1.28	90.00 ± 1.26	91.10 ± 1.27
ICO (Pct)	0.10 ± 0.04	0.40 ± 0.08	3.40 ± 0.25	5.60 ± 0.32	8.00 ± 0.38	10.00 ± 0.43	8.90 ± 0.40
Fcc (Pct)	21.10 ± 0.61	2.50 ± 0.02	0	0	0	0	0
Hcp (Pct)	13.70 ± 0.50	1.10 ± 0.14	0	0	0	0	0
Bcc (Pct)	0.60 ± 0.10	2.10 ± 0.19	—	—	—	—	—

atoms become mainly 12 and 13. However, due to their larger atomic radius, Ti-centered atoms exhibit highly coordinated clusters, with 13-, 14-, and 15-coordinated atoms being the most abundant. This result confirms that in the glassy state, the clusters are highly coordinated around the atom with the big atomic radius. Similar behavior was observed in the specific compositions $Mg_{61}Cu_{28}Gd_{11}$, $Cu_{64}Zr_{36}$, and $Pd_{82}Si_{16}$ MGs.[35,41]

C. *Voronoi Tessellation Analyses*

VTA provide a good technique for exploring local structure at short-range distances. This method was used here to investigate the distribution of major and common types of clusters that can be found in each composition of Ti-Al MGs. In MGs, the most prominent VPs are classified into three main groups.[42] The

Table II. Partial and Total CNs in Al-Ti MGs

Alloys	CN_{Al-Al}	CN_{Al-Ti}	CN_{Ti-Ti}	CN_{Ti-Al}	CN_{Al}	CN_{Ti}	CN_{all}
$Ti_{85}Al_{15}$	1.11	11.47	10.76	1.90	12.58	12.66	12.65
$Ti_{75}Al_{25}$	2.07	10.78	9.53	3.52	12.85	13.05	13.00
$Ti_{62}Al_{38}$	3.48	9.19	7.68	5.74	12.67	13.42	13.14
$Ti_{50}Al_{50}$	4.96	7.67	6.12	7.58	12.63	13.70	13.17
$Ti_{37}Al_{63}$	6.84	5.81	4.11	9.94	12.65	14.05	13.17
$Ti_{25}Al_{75}$	8.50	4.29	2.40	12.02	12.79	14.42	13.20
$Ti_{10}Al_{90}$	10.94	2.05	0.45	14.37	12.99	14.82	13.17

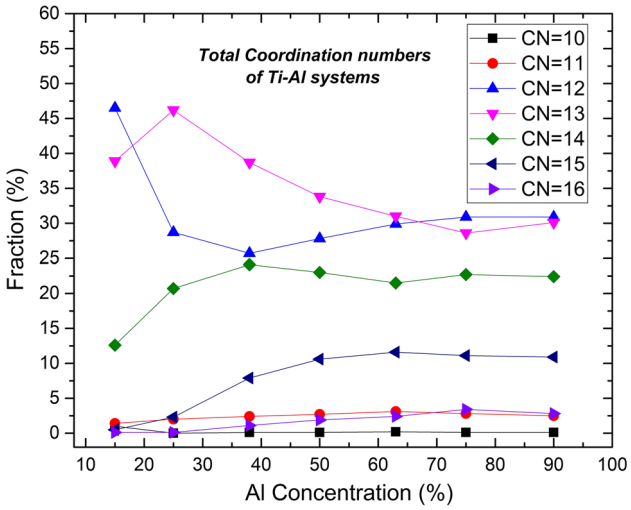

Fig. 2—Distribution of major CNs in the Ti-Al MGs at 300 K as a function of Al composition.

first group of VPs indexed by ⟨0, 0, 12, *x*⟩, ⟨0, 1, 10, *x*⟩, and ⟨0, 2, 8, *x*⟩ (where *x* is usually between 0 and 4) with approximate fivefold rotational symmetry are called "icosahedral-like." Then the VPs indexed by ⟨0, 3, 6, *x*⟩, representing the "mixed" group, and the last VP group ⟨0, 4, 4, *x*⟩, ⟨0, 5, 2, *x*⟩, and ⟨0, 6, 0, *x*⟩ with rectangular or hexagonal faces along fourfold and sixfold rotational symmetry are called "crystal-like."

Among the various polyhedra of Ti-Al systems, the Al-centered full icosahedra (FI) with Voronoi index ⟨0, 0, 12, 0⟩ constitute the most populous structural unit connected by different sharing modes (Figure 4). However, it is believed that the icosahedral-like structural order plays a major role in the vitrification of several MGs since it shows a good packing efficiency. In this article, we computed the different Voronoi clusters and divided them into three classes: the icosahedral-like, including the ideal ones with the Voronoi indices ⟨0, 0, 12, 0⟩, and the deformed units, including Voronoi indices of ⟨0, 2, 8, 2⟩, ⟨0, 2, 8, 3⟩, ⟨0, 2, 8, 4⟩, ⟨0, 1, 10, 2⟩, ⟨0, 1, 10, 3⟩, ⟨0, 1, 10, 4⟩, ⟨0, 0, 12, 3⟩, and ⟨0, 0, 12, 4⟩; the mixed polyhedral, including ⟨0, 3, 6, 3⟩ and ⟨0, 3, 6, 4⟩; and the crystal-like clusters, ⟨0, 4, 4, 4⟩. We only counted for the most abundant polyhedral, and those with fractions less than 1 pct were neglected. Therefore, the vitrification process can be regarded as the competition between icosahedral-like clusters, mixed clusters, and crystal-like clusters.

The most prominent cluster is the FI, which was found to be connected by sharing atoms in different modes. This connectivity allows determination of the MRO that describes the next level of structural networking by classifying how the SRO units are clustered in the metallic glass. The modes of connecting clusters in MGs were described in several previous works.[43,44] If two icosahedra are connected by sharing only one neighboring atom, they are recognized as vertex-sharing icosahedra (VS, Figure 5(d)). If they share two connected atoms, they are named edge-sharing icosahedra (ES, Figure 5(c)). If they share more than two connected atoms, they are defined as face-sharing icosahedra (FS, Figure 5(b)). If two icosahedra share five common neighbor atoms and the two center atoms are first neighbors to each other, they are identified as intercross sharing icosahedra (IS, Figure 5(a)). However, clusters without any sharing mode are considered as isolated polyhedra. We note that average computed distances between central atoms of the two full icosahedral clusters in Ti-Al MGs did not show any significant change with the alloy compositions. This distance between central atoms is found to be $d_{IS} = 2.86 \pm 0.15$ Å for intercross sharing, $d_{FS} = 4.78 \pm 0.15$ Å for face sharing, $d_{ES} = 5.32 \pm 0.10$ Å for edge sharing, and $d_{VS} = 5.66 \pm 0.10$ Å for vertex sharing.

In Figure 4, we plotted the PRDF curves of icosahedral atoms $g_{ico\text{-}ico}(r)$ where only central atoms of icosahedral units are considered. We deduce from Figure 4 that the first peak of the PRDF curve is related to the spatially connected intercross-sharing mode ($R_1 \approx d_{IS}$), indicating that an important amount of the clusters are linked *via* IS, which occurred most frequently. This corroborates the results of Zemp *et al.*[45] who found that the FI are predominantly connected by cap-sharing bonds and concluded that the large interconnectivity can only be achieved by a heterogeneous spatial distribution of FI. Moreover, the second peak located at ($R_2 \approx d_{FS}$) represents the face-sharing mode and the third peak ($R_3 \approx d_{VS}$) is linked to the vertex-sharing mode, whereas the edge-sharing (d_{ES}) mode is located between the second and third peaks R_2 to R_3 and should be hidden due to the overlapping between the two peaks. These results are in agreement with previous molecular dynamic simulations performed on $Mg_{70}Zn_{30}$ and Ni_3Al MGs.[43,46]

The results of the VTA are plotted in Figure 6, which shows that the fraction of the icosahedral-like polyhedra increases while the fractions of the mixed-like and the crystal-like polyhedra decrease when the Al composition

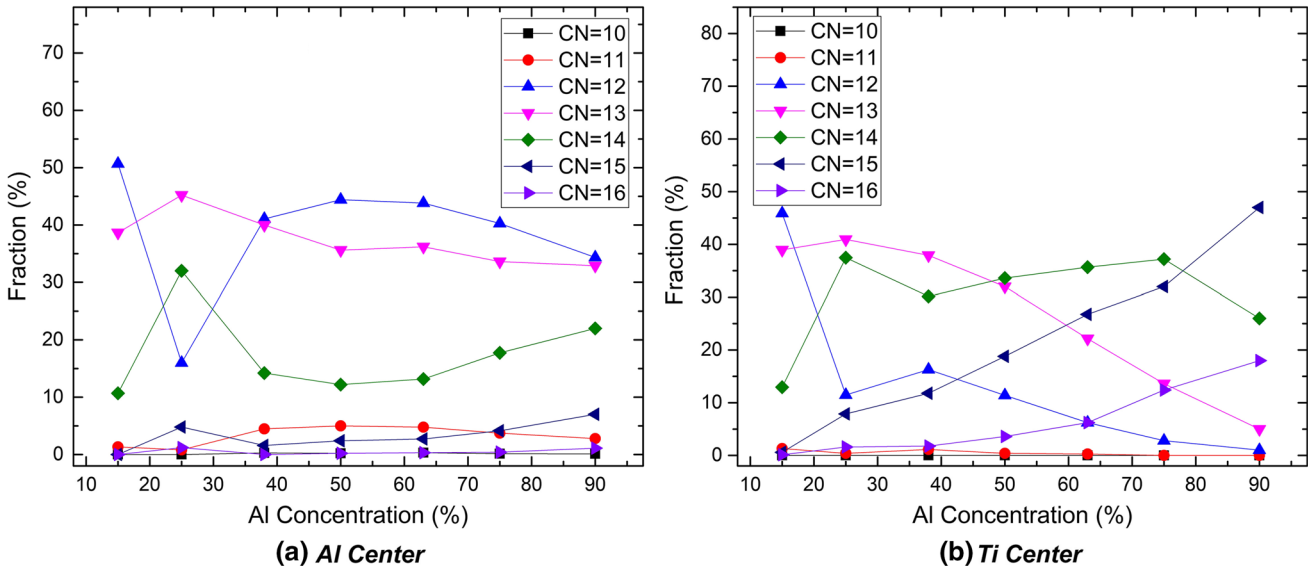

Fig. 3—Distribution of major CNs in the Ti-Al MGs at 300 K: (*a*) around Al atom centers and (*b*) around Ti atom centers.

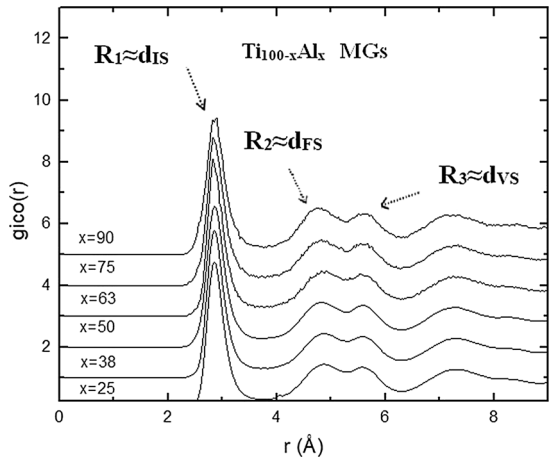

Fig. 4—Partial RDF curves of icosahedral atoms $g_{ico\text{-}ico}(r)$ between central atoms of icosahedral units in $Ti_{100-x}Al_x$ MGs, as shown in the figure.

increases up to 75 pct. However, when Al concentration exceeds 75 pct, the fraction of icosahedral-like clusters decreases because of the significant drop of the fraction of the ideal icosahedral cluster. This specific composition at 75 pct of Al content revealed the maximum amount of icosahedral-like structural polyhedral, as was also confirmed by the CNA in Section I. As these icosahedral-like clusters have a good packing factor and should contribute to the densification of the system, leading to frozen regions hindering any transformation to crystals, we suggest that in the Al-Ti system, there should be a maximum of GFA around 75 pct. Indeed, we have shown that around this value, the CNA provided the maximum fraction of the icosahedral units (Table I), the VTA led to the most important fraction of icosahedral-like clusters (Figure 6), and the coordination analysis gave a good densification of the material through an important fraction of highly coordinated atoms (Figure 2). In general, we agree with the results found in TiAl MG by Xie et *al.*,[11] where the variation of the relative amounts of the main bond types during the rapid solidification indicated an important amount of ideal icosahedral units followed by defect icosahedral ones. We should mention here that the GFA does not represent a measured parameter but is linked to a qualitative expectation from the behavior of several structural observations.

Figure 7(a) shows more details concerning the evolution of the different polyhedra involved in the Al-Ti MGs. The population of the ideal icosahedron ⟨0, 0, 12, 0⟩ cluster and the icosahedral-like clusters increases considerably in the Al-rich zone when the fraction of Al reaches 70 pct. The GFA becomes important when the fraction of Al atoms increases by forming and connecting the icosahedral-like clusters (12-coordinated ⟨0, 0, 12, 0⟩ and 13-coordinated ⟨0, 1, 10, 2⟩), so these two polyhedra play a major role in the structure stability of the Ti-Al MGs. However, when the Al composition reaches 100 pct, forming a monoatomic system, the ideal icosahedron units decrease and the GFA becomes weaker, which confirms the requirement of a multicomponent system for a good GFA.[6,7] On the other hand, at the Ti-rich zone, Figure 7(b) shows that the ⟨0, 3, 6, 3⟩, ⟨0, 4, 4, 4⟩, and ⟨0, 3, 6, 4⟩ clusters (CN = 12 and CN = 13) became the most dominant polyhedra at the expense of the ideal icosahedron. This explains why the GFA becomes weaker for high Ti concentrations. This result is in agreement with those obtained in the binary Cu-Zr MGs,[9] where it was suggested that the most dominant polyhedra for high Cu concentration are the ⟨0, 0, 12, 0⟩ and ⟨0, 1, 10, 2⟩ polyhedra. We suggest that these two polyhedra are essential clusters for an easy formation of Ti-Al MGs. We also suggest that the appearance of the non-icosahedral-like clusters at the expense of the icosahedral-like ones may occur *via* some well-defined mechanisms where the free volume migration plays an important role. This was also observed

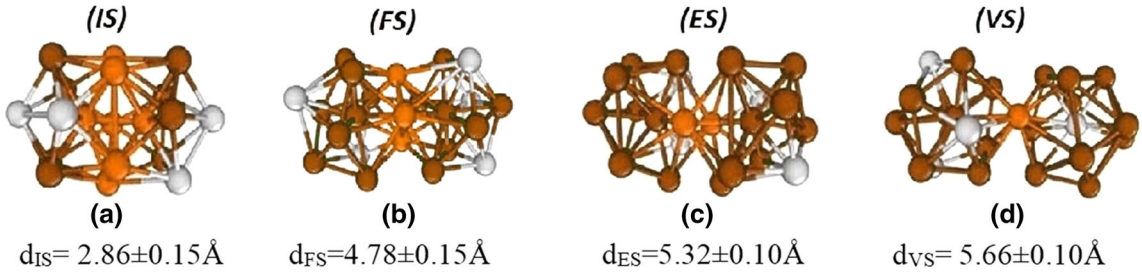

Fig. 5—Illustrations of isolated (*a*) interpenetrating and (*b*) face-, (*c*) edge-, and (*d*) vertex-sharing modes of Voronoi polyhedra in the Ti-Al MGs. *d* is the average distance between central atoms of two connected polyhedra. The brown and gray represent Al and Ti atoms, respectively. The orange balls are the sharing atoms of two polyhedra.

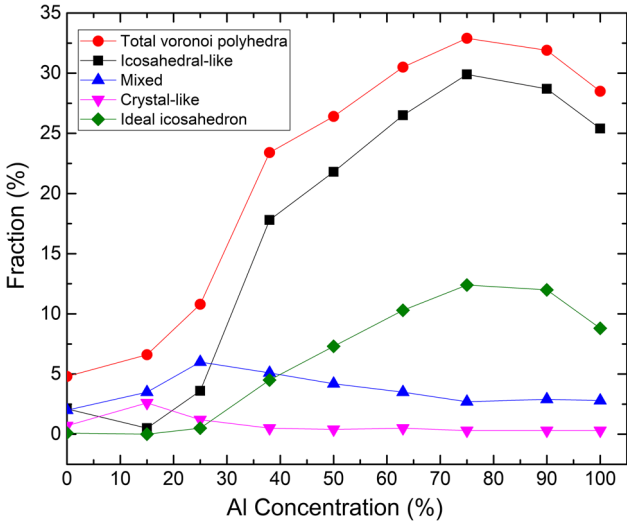

Fig. 6—Variation of the major Voronoi polyhedra, icosahedral-, mixed-, and crystal-like polyhedra with Al concentration of Ti-Al systems at $T = 300$ K.

experimentally using the Angstrom-beam electron diffraction technique,[47] where the authors confirmed the coexistence of both full and distorted icosahedra (DI) in MGs.

Further details can be reached by examining the polyhedra centered on each atom type. Figure 8(a) shows that when the Al concentration increases and exceeds 25 pct, more icosahedral structures centered on Al atoms are formed where the most dominant Al-centered polyhedra are $\langle 0, 0, 12, 0\rangle_{CN=12}$ and $\langle 0, 1, 10, 2\rangle_{CN=13}$. However, Figure 8(b) shows that the most dominant Ti-centered polyhedra are $\langle 0, 3, 6, 4\rangle_{CN=13}$ at the Ti-rich zone and $\langle 0, 2, 8, 4\rangle_{CN=14}$ with $\langle 0, 0, 12, 3\rangle_{CN=15}$ at the Al-rich zone. Nevertheless, the maximum fraction of the most abundant of these polyhedra did not exceed 2.7 pct, and this is a weak fraction compared to those centered on Al atoms. We should note that the fraction of $\langle 0, 0, 12, 0\rangle$ VP is almost 12 pct in $TiAl_3$ alloy, while for pure Al, it is almost 8 pct, which is yet higher than other studied compositions located mainly at the Ti-rich zone. However, the GFA of pure Al glass is known to be very low, which is in discrepancy with our suggestion that icosahedral order correlates with high GFA. This discrepancy may be due to very high cooling rates used in general in MD simulations, which can promote vitrification of monoatomic systems.[24,44]

Therefore, we conclude from the cluster atomic configuration examined by the CN technique and the VTA that Ti atoms like to contribute to the formation of Al-centered icosahedral clusters or to bring together atoms (Al or Ti) to form larger centered Ti polyhedra indexed as $\langle 0, 2, 8, 4\rangle_{CN=14}$ or $\langle 0, 0, 12, 3\rangle_{CN=15}$. Indeed, larger atoms tend to have more topological coordination,[13,41] which should occur for Ti atoms due to their larger radius ($R_{Ti} = 1.76$Å, $R_{Al} = 1.18$Å), leading to an expansion of the cluster volume.[41] Moreover, topologically atomic configurations of nearest neighbors in the first shell (Figure 3) revealed that the clusters are highly coordinated around the larger atom. In light of our results and those obtained using MD simulations of $Cu_{64}Zr_{36}$ MGs,[45] we suggest that the FI $\langle 0, 0, 12, 0\rangle$ is the most dominant cluster followed by other DI.

IV. CONCLUSIONS

We have studied a large range of compositions of Ti-Al amorphous alloys by employing MD simulations with EAM many-body potential. Total RDFs and PRDFs for the Ti-Ti, Al-Al, and Ti-Al atom pairs have been computed for different compositions and illustrated the formation of the icosahedral structure by the splitting of the second peak, a notable characteristic of a metallic glass. Then the presence of icosahedral units was confirmed by CNA, which shows a more pronounced fraction of icosahedral at the $Ti_{25}Al_{75}$ composition. According to the CNs analysis, Al atoms are mainly 12 and 13 coordinated and Ti atoms exhibit highly coordinated atoms with 13, 14, and 15 coordination, due to their larger atomic radius. Ti atoms are expected to connect to each other as neighboring atoms in Al-centered icosahedral clusters or to assemble larger polyhedra at high Al concentrations. Our results show that the highest number of icosahedra is obtained at 75 pct of Al concentration. This specific composition represents a peritectic point localized at a low melting point in the binary phase diagram of the Ti-Al system and can be added to the conditions of GFA[6] for forming good MGs, though we propose this prediction should be verified by future experiments.

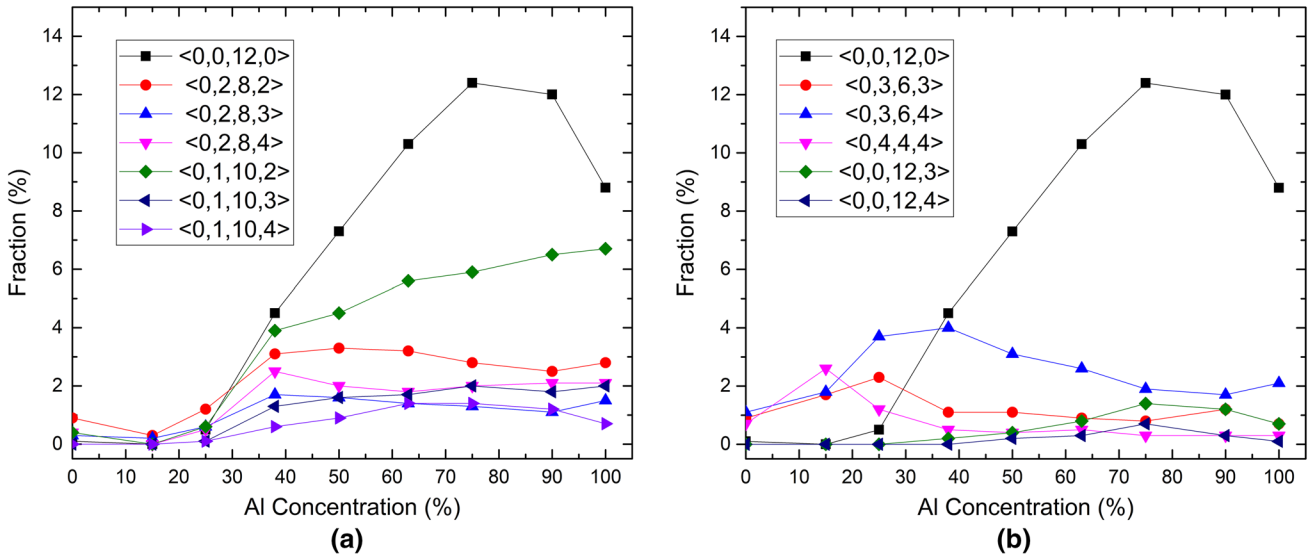

Fig. 7—Variation in the population of major Voronoi polyhedra with Al concentration in the Ti-Al glass at $T = 300$ K: (*a*) icosahedral-like polyhedra and (*b*) crystal- and mixed-like clusters.

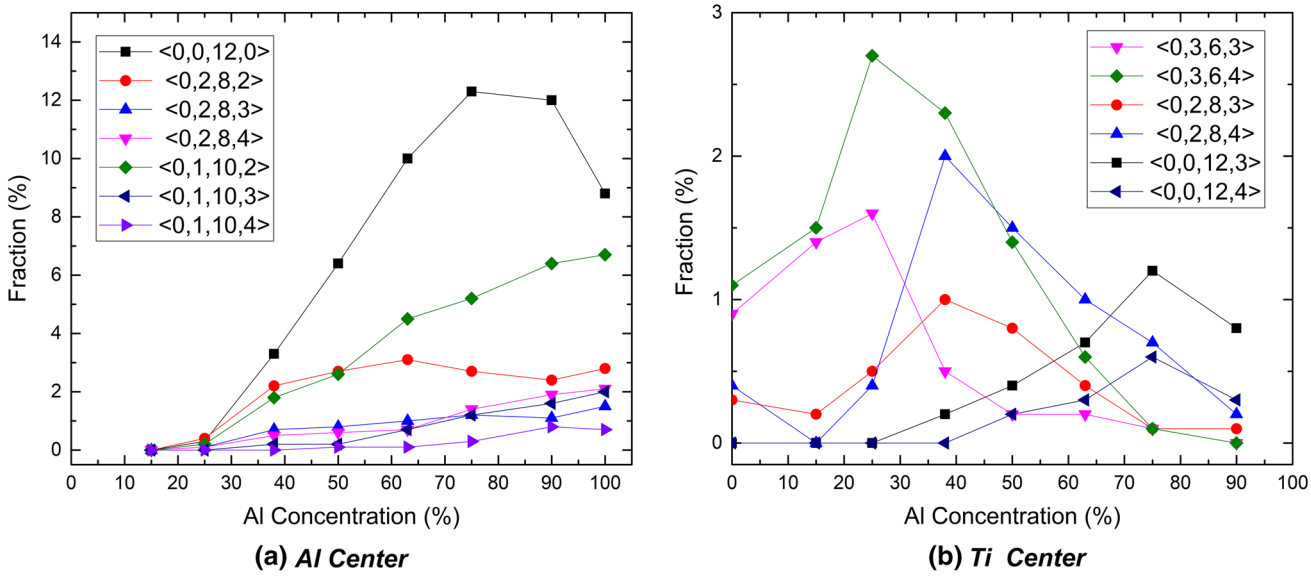

Fig. 8—Population of the major Voronoi polyhedra as a function of Al concentration in the Ti-Al MGs at $T = 300$ K, centered around (*a*) Al atoms and (*b*) Ti atoms.

We conclude that the GFA becomes important when the fraction of Al atoms increases by forming and connecting icosahedral-like clusters (12-coordinated ⟨0, 0, 12, 0⟩ and 13-coordinated ⟨0, 1, 10, 2⟩), so they are essential clusters for an easy formation of Ti-Al MGs.

ACKNOWLEDGMENT

We thank Professor S. El Yamani, Hassan 1st University, for editing our article by refining the style and English language of the manuscript.

REFERENCES

1. A.H. Inoue, A. Kato, T. Zhang, S.G. Kim, and T. Masumoto: *Mater. Trans. JIM*, 1991, vol. 32, pp. 609–16.
2. D.H. Xu, G. Duan, and W.L. Johnson: *Phys. Rev. Lett.*, 2004, vol. 92, p. 245504.
3. T. Masumoto and R. Maddin: *Acta Metall.*, 1971, vol. 19, pp. 725–41.
4. H.S. Chen: *Rep. Progr. Phys.*, 1980, vol. 43, pp. 353–432.
5. M.F. Ashby and A.L. Greer: *Scripta Mater.*, 2006, vol. 54, pp. 321–26.
6. A. Inoue: *Acta Mater.*, 2000, vol. 48, pp. 279–306.
7. J.H. Li, Y. Dai, Y.Y. Cui, and B.X. Liu: *Mater. Sci. Eng. R.*, 2011, vol. 72, pp. 1–28.
8. C.C. Wang and C.H. Wong: *J. Alloys Compds.*, 2011, vol. 509, pp. 10222–29.

9. H.L. Peng, M.Z. Li, W.H. Wang, C.Z. Wang, and K.M. Ho: *Appl. Phys. Lett.*, 2010, vol. 96, p. 021901.
10. Z.C. Xie, T.H. Gao, X.T. Guo, and Q. Xie: *J. Non-Cryst. Solids*, 2014, vol. 406, pp. 95–101.
11. Z.C. Xie, T.H. Gao, X.T. Guo, X.M. Qin, and Q. Xie: *Physica B*, 2014, vol. 440, pp. 130–37.
12. Z.C. Xie, T.H. Gao, X.T. Guo, X.M. Qin, and Q. Xie: *Comput. Mater. Sci.*, 2014, vol. 95, pp. 502–08.
13. C.C. Wang and C.H. Wong: *J. Alloys Compds.*, 2012, vol. 510, pp. 107–13.
14. H. Chen, Y. He, G.J. Shiflet, and S.J. Poon: *Scripta Metall. Mater.*, 1991, vol. 25, pp. 1421–24.
15. Y.H. Kim, A. Inoue, and T. Masumoto: *Mater. Trans. JIM*, 1991, vol. 32, pp. 331–38.
16. Y. He, S.J. Poon, and G.J. Shiflet: *Science*, 1988, vol. 241, pp. 1640–42.
17. S.D. Zhang, Z.M. Wang, X.C. Chang, W.L. Hou, and J.Q. Wang: *Corros. Sci.*, 2011, vol. 53, pp. 3007–15.
18. N.C. Wu, L. Zuo, J.Q. Wang, and E. Ma: *Acta Mater.*, 2016, vol. 108, pp. 143–51.
19. G. Chen, W. Zhang, Z. Liu, S. Li, Y. Kim, Y. Kim, D. Dimiduk, and M. Loretto: *Gamma Titanium Aluminides*, TMS, Warrendale, PA, 1999, p. 371.
20. F. Appel, U. Brossmann, U. Christoph, S. Eggert, P. Janschek, U. Lorenz, J. Müllauer, M. Oehring, and J.D. Paul: *Adv. Eng. Mater.*, 2000, vol. 2, pp. 699–720.
21. P.C. Priarone, S. Rizzuti, L. Settineri, and G. Vergnano: *J. Mater. Process. Technol.*, 2012, vol. 212, pp. 2619–28.
22. J. Aguilar, A. Schievenbusch, and O. Kättlitz: *Intermetallics*, 2011, vol. 19, pp. 757–61.
23. E.V. Levchenko, A.V. Evteev, G.G. Löwisch, I.V. Belova, and G.E. Murch: *Intermetallics*, 2012, vol. 22, pp. 193–202.
24. M. Tahiri, S. Trady, A. Hasnaoui, M. Mazroui, K. Saadouni, and K. Sbiaai: *Mod. Phys. Lett. B*, 2016, vol. 30, p. 1650170.
25. M. Tahiri, A. Hassani, A. Hasnaoui, and K. Sbiaai: *J. Comput. Condens. Matter*, 2018, vol. 14C, pp. 74–83.
26. S. Plimpton: *J. Computat. Phys.*, 1995, vol. 117, pp. 1–19.
27. *LAMMPS Users Manual,* Sandia National Laboratories, Albuquerque, NM, 2014, http://lammps.sandia.gov/.
28. S. Nose: *Mol. Phys.*, 1984, vol. 52, pp. 255–68.
29. M.S. Daw and M.I. Baskes: *Phys. Rev. B*, 1984, vol. 29, pp. 6443–53.
30. M.S. Daw and M.I. Baskes: *Phys. Rev. Lett.*, 1983, vol. 50, pp. 1285–88.
31. R.R. Zope and Y. Mishin: *Phys. Rev. B*, 2003, vol. 68, p. 024102.
32. A.S. Clarke and H. Jónsson: *Phys. Rev. E*, 1993, vol. 47, pp. 3975–84.
33. D. Faken and H. Jónsson: *Comput. Mater. Sci.*, 1994, vol. 2, pp. 279–86.
34. L. Wang, Y. Zhang, H. Yang, and Y. Chen: *Phys. Lett. A*, 2003, vol. 317, pp. 489–94.
35. Y.Q. Cheng, J. Ding, and E. Ma: *Mater. Res. Lett.*, 2013, vol. 1, pp. 3–12.
36. Y.Q. Cheng and E. Ma: *Progr. Mater. Sci.*, 2011, vol. 56, pp. 379–473.
37. G.Q. Guo, S.Y. Wu, S. Luo, and L. Yang: *Metals*, 2015, vol. 5, pp. 2093–2108.
38. H.W. Sheng, W.K. Luo, F.M. Alamgir, J.M. Bai, and E. Ma: *Nature*, 2006, vol. 439, pp. 419–25.
39. D.B. Miracle: *Nat. Mater.*, 2004, vol. 3, pp. 697–702.
40. R. Soklaski, Z. Nussinov, Z. Markow, K.F. Kelton, and L. Yang: *Phys. Rev. B*, 2013, vol. 87, p. 184203.
41. X.D. Wang, H.B. Lou, S.G. Wang, J. Xu, and J.Z. Jiang: *Appl. Phys. Lett.*, 2011, vol. 98, p. 031901.
42. P. Zhang, J.J. Maldonis, M.F. Besser, M.J. Kramer, and P.M. Voyles: *Acta Mater.*, 2016, vol. 109, pp. 103–14.
43. Y.C. Liang, R.S. Liu, Y.F. Mo, H.R. Liu, Z.A. Tian, Q. Zhou, H.T. Zhang, L.L. Zhou, Z.Y. Hou, and P. Peng: *J. Alloys Compd.*, 2014, vol. 597, pp. 269–74.
44. S. Trady, M. Mazroui, A. Hasnaoui, and K. Saadouni: *J. Non-Cryst. Solids*, 2016, vol. 443, pp. 136–42.
45. J. Zemp, M. Celino, B. Schonfeld, and J.F. Loffler: *Phys. Rev. B*, 2014, vol. 90, p. 144108.
46. S. Trady, M. Mazroui, A. Hasnaoui, and K. Saadouni: *J. Non-Cryst. Solids*, 2017, vol. 468, pp. 27–33.
47. A. Hirata, L.J. Kang, T. Fujita, B. Klumov, K. Matsue, M. Kotani, A.R. Yavari, and M.W. Chen: *Science*, 2013, vol. 341, pp. 376–79.